Effects of groundwater table on buried pipeline response to a surface explosion

Mohammad T. Ahmadi[a] and F. Ershadi[a]*

[a] *Civil and Environmental Engineering Dept., Tarbiat Modares University, Tehran, Iran*

P A P E R I N F O

Paper history:
Received
Received in revised form
Accepted

Keywords:
Buried pipeline
Explosion
Groundwater table
Finite element method
Pipe-Soil Interaction

A B S T R A C T

Groundwater table is a fluctuating factor changing soil structure and affecting pipes' response to any load, such as an explosion. After validation with the results of previous studies, several numerical models were elaborated with ten different groundwater levels and two states of 1. Empty, 2. Pressurized for a buried pipe to investigate this for an explosion load. These simulations were solved by a Finite Element Method (FEM) solver. This research only studies the effects of non-cohesive soils and neglects the semi-saturated part of the soil for simplicity. The pipe's effective stress and plastic strain in each scenario were studied. The results state that the most critical scenario is when the water table is around the pipe crown, whether the pipe is empty or pressurized, with considerable excess stress compared to the absence of groundwater table. The deformation mode is also hugely affected by the water table, changing from local, forming a dent, to non-local. The internal pressure of the pipe also considerably reduces the pipe stresses and strains whether the surrounding soil is saturated or dry. Such results are certainly impactful in efficiently designing buried pipelines, which most existing guidelines and codes have not considered.
doi:

1. INTRODUCTION

Using buried pipelines has become a popular way to transport in oil and gas industries, especially in terms of reliability and security. However, accidental explosions, such as quarries, public works, open-pit mines, or even intentional explosions, can threaten such pipelines. Some blasting terrorist attacks have also happened, such as in London (2005) and Chechnya (2002). These explosions not only can cause considerable damage to people's lives and property, but they can also be a threatening factor in damaging buried pipelines, which affects the safety of a large community. Therefore, studying the dynamic response of buried pipelines under surface explosions is essential for either constructing new ones or evaluating existing ones.

There are several studies investigating the response of structures under explosive loads. Lu et al. compared the response of a buried reinforced concrete structure to an underground explosive charge in 2-dimensions and 3-dimensions, using the Smooth Particle Hydrodynamics (SPH) coupled with the Finite Element Method (FEM) [1]. Fiserova, both numerically and experimentally, investigated the effects of soil properties on buried mine explosives [2]. Such properties included different soil types, varying moisture content and some factors relating to the explosive. The static and dynamic responses of underground pipelines under an internal explosion were examined by Olarewaju et al. [3]. Song et al. studied the response of an X70 pipeline subject to localized explosion loading, both experimentally and numerically and found different failure modes [4]. They also found that the wall thickness of the pipe is an influential factor in damage and post-failure motion.

Guo et al. [5] numerically studied the safety spacing of underground parallel gas pipelines in the case of exploding one of the pipelines. The effects of ground surface blasting on a buried gas pipeline were discussed in other studies [6], [7]. It was based on a case study in Wuhan, China, and the researchers used experimental field data to validate their numerical simulation. Subsequently, they analyzed the pipeline's response, and the safety area for explosion parameters was obtained. Kontogeorgos et al. [7] studied and reported the meta-material application to protect underground gas transmission pipelines. They found the implementation of meta-materials for the blast protection of underground structures efficient. Telichenko et al. [8] developed a numerical model to study the groundwater pressure distribution in the vicinity of underground structures. Their study included the effects of different parameters such as the aquifer thickness, the filtration coefficient, the soil porosity, the piezoelectric conductivity coefficient and the viscosity coefficient.

Zhang et al. performed detailed research on an underground pipe affected by a surface explosion, with different eccentric explosions, explosive distances, charge weights and burial depths, using the FEM method [9]. Although research uses more complicated soil models to model saturated soils in an explosion scenario [10]–[12], subjecting such conditions to a buried pipeline remains unanswered, especially in a surface explosion case.

This paper investigates the effects of the groundwater table on a buried pipeline due to a surface explosion, using the commercial code LS-DYNA,

*Corresponding Author Email: f.ershadi@modares.ac.ir

which conducts FEM simulations. An Eulerian solver was used

to model TNT, air, soil and water inside the pipe. The lagrangian solver was used for the pipe. This appears to be an appropriate approach to model high deformations in air and soil, while the required accuracy for pipe elements and their stresses are to be achieved. The methodology and the model approach are initially verified with Zhang's study's reported results [9]. Consequently, the pipe response for different groundwater tables is presented and discussed.

2. GOVERNING EQUATIONS

There are some nonlinear material models alongside Equations Of State (EOS) to model the material behaviours in this study. These models and equations are explained in detail in the following.

Before the explosion, the material model of TNT can be explained as Jones-Wilkins-Lee (JWL) model and EOS [13]. After the explosion, a gaseous property is presented for the TNT explosive, using the JWL as its equation of the state. This equation of state describes the pressure that the expansion of explosive products generates through the chemical reaction. Its equation is as follows [13]:

$$P = A(1-\frac{\omega}{R_1})e^{-R_1V} + B(1-\frac{\omega}{R_2V})e^{-R2V} + \frac{\omega E}{V} \quad (1)$$

P presents pressure, E presents the internal energy per unit volume of TNT, V is the TNT relative volume. A, B, ω, R_1 and R_2 are the equation constants determined for conventional explosives through dynamic experiments. These values and other needed ones for the TNT explosive are shown in **Table 1.**

ρ presents the material density, v_D presents the detonation velocity and P_{CJ} is the Chapman-Jouget pressure for the TNT. E_0 is the detonation energy per unit volume. All of these parameters are used in modelling the explosion waves.

The material model used for air ignores the computation of deviatoric stresses. This material model requires an equation of state. The linear polynomial EOS was used for this purpose, which calculates the pressure as follows [14]:

$$P = C_0 + C_1\mu + C_2\mu^2 + C_3\mu^3 + (C_4 + C_5\mu + C_6\mu^2)E \quad (2)$$

$$\mu = \frac{1}{V} - 1 = \frac{\rho}{\rho_0} - 1 \quad (3)$$

Where P, E, E_0, ρ and V were the same parameters that were described before. The rest of the parameters are the constants of this equation ($C_0 - C_6$). ρ_0 is the density in nominal/reference state. To comply gamma law for modelling air with this equation of state, the constant values and other required ones are given in **Table 2** are used.

For modelling water inside the pipe in scenarios with internal water pressure, the Gruneisen EOS is used. This EOS defines pressure in compressed materials using the equation below [14].

$$P = \frac{\rho_0 C'\mu(1+(1-\frac{\gamma_0}{2})\mu - \frac{a}{2}\mu^2)}{[1-(S_1-1)\mu - S_2\frac{\mu^2}{\mu+1} - S_3\frac{\mu^3}{(\mu+1)^2}]^2} + (\gamma_0 + a\mu)E \quad (4)$$

Where $\acute{C}$ is the intercept of particle and shock wave velocity curve velocity, S_1, S_2 and S_3 are the coefficients defined by the u_p-u_s curve slope. The Gruneisen gamma is γ_0, and a is the correction of first order to γ_0. These parameters for modelling water are shown in **Table 3**.

The material model of the pipe should be able to consider strain rate, as explosions induce a high strain rate on the pipe. For this reason, the simplified Johnson-Cook model was used to model the pipe's behaviour. This model includes strain hardening and strain rate effects in its simulations, which can improve accuracy. Its formulation is as follows [14]:

$$\sigma_y = (A' + B'\bar{\varepsilon}^{p^n})(1 + c\ln\dot{\varepsilon}^*) \quad (5)$$

In which $\bar{\varepsilon}^p$ and $\dot{\varepsilon}^*$ are the equivalent plastic strain and effective strain rate, respectively. The other parameters are the model constants. This model simulates X70 steel, a low-carbon alloy steel commonly used for pipelines. This steel has continuous yield characteristics with high elongation. However, it has no significant yield platform. This model is used in the main calculations of this research. The parameters used for this model are shown in **Table** 4.

To simplify the problem, two types of soil are required. One is needed for the soil above the groundwater table, the dry one and another model for the saturated soil located under the groundwater table. In other words, the soil layers between these two types of soil are assumed to have little to no effect on the pipe response to the explosion.

The mechanical behaviour of dry soil is modelled with the Mohr-Coulomb material model. This model is characterized by the elastic modulus E, the cohesion c, the friction angle φ and Poisson ration v. For this study, the dilation angle is set to zero. The used parameters for the dry soil are shown in **Table 5.**

To model the saturated sand, however, another model was used by the name of FHWA, which was established by Lewis (1999) for the Federal Highway Administration (FHWA) [15]. This decision was because this model includes kinematic hardening, strain softening, element deletion, strain rate effects, and, most

importantly, the effects of excess pore water pressure [14]. Besides, several studies have adopted this model to simulate soil dynamic response to blast loads [11], [12], [16].

The FHWA model is based on the Mohr-Coulomb criterion, proven to model soil behaviour concisely and efficiently. A smooth hyperbolic surface is adopted in this model to overcome numerical problems that the singularity at the yield surface intersection and pressure axis cause, which is shown in **Figure 1**.

In this yield criterion, *Ahyp* controls how close the modified surface and the standard Mohr-Coulomb yield criterion is, *P* accounts for pressure, φ stands for the internal friction angle, *K(θ)* is the function of the Lode angle θ, *C* is the cohesion, and J_2 is the stress deviator second invariant.

The strain rate effect is included by interpolating elastic trial stress and inviscid stress using the Devaut-Lions two-parameter visco-plastic update algorithm. The presented formula shows the inviscid stress.

$$\bar{\sigma}_{vp} = (1-\zeta)\bar{\sigma} + \bar{\sigma}_{trail} \quad (6)$$

In which $\zeta = 1/(\Delta t/\eta + 1)$, and $\eta = (\gamma/\dot{\varepsilon})^{\frac{N-1}{N}}$. The parameter γ adjusts the viscosity, and *N* is its exponent. The input card for saturated sand is given in **Table 6**.

In **Table 6,** ρ represents the density of the soil material. G_s stands for the specific gravity of the saturated soil, and ρ_{water} is the density of the water. *N* and γ are viscosity parameters used to develop strain-rate-enhanced strength for the material model and are described before, along with *K* and *G*. *Itermax* is the maximum number of plasticity iterations. Φ_{max} is the peak friction angle used in the Mohr-Coulomb failure criteria calculations. *e* is the eccentricity parameter used for the third stress invariant effects. A_n is the percentage of Φ_{max} in which nonlinear behaviour begins, while E_t is the desired measure of the nonlinear strain hardening effects. m_c shows the moisture content of the soil. D_1 is the parameter that controls the soil stiffness before the air voids collapse, and K_{sk} is the non-porous bulk modulus of the soil. D_2 is another parameter modifying the effective pressure due to pore water effects. D_1, D_2 and K_{sk} are used to modify the bulk modulus of the soil due to considering pore water effects. Φ_{res} presents the slope of the failure surface in radians. ε_0 is the strain at

$$\sigma_{normal} = \varphi c_d V_{normal} \quad (7)$$

$$\sigma_{shear} = \varphi c_{sh} V_{\tan} \quad (8)$$

which the damage starts. Also, G_f is similar to fracture energy in metals that, in this model, is used to calculate the strain at full damage. *Damlev* is the percentage of the damage which causes the element deletion. ε_{max} is also the maximum principal strain at which an element is deleted. Detailed explanations about the material model and its parameters can be found in Ref. [14].

The buried pipeline is modelled with solid elements in four layers in the radial direction and solved by the Lagrangian algorithm. It is solved with 8 Gauss points. Due to the poor aspect ratio of the elements, there is a modification to the Jacobian matrix to reduce the spurious stiffness without affecting the physical behaviour of the elements [17]. Other parts such as

$$F = -P\sin\varphi + \sqrt{J_2 K(\theta)^2 + Ahyp^2 \sin^2\varphi} - C\cos\varphi \quad (9)$$

TNT, soil, water and air are simulated with solid elements and solved by the one-point Eulerian algorithm. These Eulerian parts connect through shared nodes so that the explosion wave can travel from one medium to another.

Due to the model's symmetry, only a quarter of it is simulated. Hence, two symmetry planes of XOY and YOZ, as shown in **Figure 2**. The top surface of the model is the free surface, which is the air boundary. However, a transmitting boundary is used for the rest of the boundaries. This type of boundary is based on the work of Lysmer and Kuhlemeyer (21), in which viscous normal and shear stresses are applied to the boundaries' outer surface. These stress are:
where c_d, c_{sh} and ρ are the dilatational wave speed, the shear wave speed and the material density. These stresses are proportional to the velocities in the normal, V_{normal}, and tangential, V_{tan}, directions. These parameters are calculated for each boundary element to prevent wave reflections from these boundaries

The contact between the pipe and surrounding soil is modelled using the Fluid-Structure Interaction algorithm. In this algorithm, the soil and the pipe acts as fluid and structure, respectively. In every time step, the penetration of the soil medium to the pipe body is calculated. Then the forces, based on the direction and the amount of penetration, are applied to the pipe and the fluid elements. This should prevent leakage and simulate the dynamics of interaction. This algorithm is called penalty-coupling as well. The penetration ratio to the applied force is achieved through try and error to optimize the validation results. **Figure 3** shows a schematic view of this algorithm in 2D. It should be noted that these forces are both in the tangential and normal directions. The interaction of the pipe and the water inside it, simulated in some of the cases explained in the next sections, are the same as pipe-soil interaction

The time step for this modelling is the minimum time step (Δt) obtained from all elements. Time steps are calculated by a fraction of The Courant–Friedrichs–Lewy (CFL) parameter. The suggested fraction is 0.67 for simulating explosions and transmitting boundaries (22). However, due to stability reasons, the factor of 0.5

is used. In this way, not only is the CFL condition satisfied but the stability and accuracy are not degraded. The CFL parameter is computed by dividing characteristic length L_e by a function of the bulk viscosity coefficients D_0 and D_1 and the adiabatic sound speed c_s. The equations below show how the CFL parameter is calculated.

$$\Delta t = \frac{L_e}{Q + (Q^2 + c_s^2)^{1/2}} \tag{10}$$

$$Q = \begin{matrix} D_1 + D_0 L_e \left|\dot{\varepsilon}_{kk}\right| & \dot{\varepsilon}_{kk} < 0 \\ 0 & \dot{\varepsilon}_{kk} \geq 0 \end{matrix} \tag{11}$$

In equations (10) and (11), Q is a function of the bulk viscosity, and ε_{kk} is the bulk strain rate. Moreover, the characteristic length, L_e, is calculated by dividing element volume by the element's maximum surface area. Given all of these equations, the initial time step is 0.1112 milliseconds. Certainly, there might be calculation steps in which the time step drops even lower, but it is still in the order of 0.1 milliseconds.

3. MODEL VALIDATION

There are many empirical relations and experiments for explosions in air media, such as Brode (1959), Henrych (1979), Baker (1974) and Wu and Hao (2005) [18]. In order to verify the explosion load, a comparison was made for the maximum explosion overpressure between the numerical results and some of these empirical relations.

Figure 4 compares the maximum overpressure of the explosion from some of these empirical results and the numerical simulation of this study. The explosion shock wave is usually expressed by scaled distance ($\bar{R}$), which is the horizontal axis of this graph. This parameter is defined as follows:

$$\bar{R} = \frac{R}{W^{1/3}} \tag{12}$$

where R is the distance from the explosive centre to the measurement point in meters, and W is defined as the TNT equivalent weight in kg.

Figure 4 illustrates that the numerical results are consistent with the overall trend of the experimental results, decreasing the overpressure peak value with increasing scaled distance. Since the empirical formulas are obtained from different explosion tests, the explosive performance and explosion types vary in different formulas. This figure explains the differences in the overpressure peaks.

As shown in **Figure 4**, the overpressure peak and error are reduced with increasing scaled distance. Since the pipe is located at larger scaled distances, the numerical results are accurate and reliable. Overall, the simulation results are less than the empirical formulas and are close to Baker and Henrych formulas.

Also, a model similar to Ref. [9] was developed to verify the shock wave propagation through soil media, pipe-soil interaction and structural performance. Regarding this, the geometrical characteristics of the current model are the same as Ref. [9]. The whole model dimensions are 5m × 4.8m × 10m in *X*, *Y* and *Z* directions, respectively. The pipe diameter is 813mm, and its burial depth is 1m. The wall thickness of the pipe is 10mm. To decrease the calculation time, symmetry boundaries in x and z directions are used. The TNT model is rectangular with 0.5m × 0.25m × 0.5m in *X*, *Y* and *Z* direction, respectively. The height of this explosive is 0.3m from the ground, and considering this position for the TNT was for verification purposes in Ref. [7]. A schematic view of the model is shown in **Figure 5**.

The results for pipe elements right below the explosion are selected for validation. These elements are located on the top (**Figure 6)**, spring-line (**Figure 7)** and bottom (**Figure 8**) of the pipe. Grid convergence is also examined during these verifications and can be seen in these figures. The number of elements in Main mesh is 97132, and that of Coarse and Fine mesh is 77238 and 121338 elements, respectively.

As shown in **Figure 6**, the effective stresses in the top element of the pipe in different element sizes compared with the Ref. [7] results are close. While all of the numerical results of this study cover the first peak, Main and Coarse mesh show better results than Fine mesh. This can be illustrated in 23ms, where the third peak of 750MPa happened for the result in Zhang et al.study.

The effective stress in these models for the pipe spring-line element is compared in **Figure 7**. In this graph, all three models almost cover the first peak of 540MPa in the Zhang et al. study. However, the results for Fine mesh after 15ms are higher than that of Coarse and Main mesh.

In **Figure 8**, the bottom element results are compared with the result reported in Ref. [9]. These models fall short by almost 100MPa from the verification result in the first peak. Nevertheless, this gap is almost closed for the second and third peaks. Still, Main mesh seems to be a better fit for the post-peak than the other two meshes.

Regarding these comparisons, Main mesh seems to result in an appropriate concordance with the results in Zhang's study; hence it is used as a reliable basis for this research.

4. NUMERICAL MODEL

The same model used for verification is used to investigate the effects of groundwater table on the pipe

response to an explosion since it converted good results.

There are ten different assumed scenarios for the groundwater elevation starting below the pipe to the ground surface. This can be seen in **Figure 9**. In this figure, Case A is where the water table is at the ground surface. The rest of the Cases are defined by the groundwater depth shown beside them, such as Case J with the groundwater table 2.3m below the ground surface.

Two different soil types are defined at these depths using two material models. Above a certain depth from the ground surface is dry sand, modelled with the Mohr-Coulomb yield criterion and parameters in **Table 4**. Below that depth is saturated sand modelled with the FHWA model explained in section 2. Its parameters are shown in **Table 5**. The soil is assumed to be granular, so the capillary effect can be neglected, leading to a simpler model. The TNT size and model are the same as the model used in verification, which equals 100Kg of TNT.

These Cases have been defined for an empty pipe and a pipe with 1 MPa internal water pressure. A more rigorous study on the effects of internal pressure was done by Zhang et al. [19]. A pre-run was established to apply the internal pressure to the pipe and the whole model to find the stresses and strains in the pipe, soil, and water inside the pipe. Then, the explosion and its effects were simulated.

5. RESULTS AND DISCUSSION

The maximum effective plastic strains for Cases with pressurized pipe were less than 0.25%, which is negligible to those of empty pipe Cases. This was expected as the internal pipe pressure helps to protect the integrity of the pipe. **Figure 10** shows these measures for the ten Cases with the empty pipe. Case D has the highest plastic strain of 11.87%, followed by Case E with 10.3%. In Case D, the groundwater table is at the top of the pipe, while it is 20cm lower in Case E. This is most likely due to the difference between the shockwave propagating through dry and saturated sand. In Cases D and E, the top of the pipe, one of the most vulnerable parts, is subjected to explosion wave travelling in the dry sand as the more potent media than saturated sand. This explains the dent in these Cases, while the rest of the pipe remained unchanged. By looking at the deformation in Cases A to C, which is non-local, this can be concluded that the groundwater table above the buried pipe makes the pipe's response non-local and can be a protective factor. Whereas in other Cases, the pipe significantly loses its ovality. In Cases H to J, although the effective plastic strain is not as high as in Case D, the formed dent is much deeper than that of Case D. This can be because of the lower resistance for the pipe to settle in Cases H to J since the soil surrounding the pipe is dry and loose. In these Cases, when the explosion shock wave reaches the pipe, a dent starts to form while this shock pushes the pipe deeper. However, in Cases D, E and F, the soil surrounding the pipe is mostly saturated and resists the settlement of the pipe, hence more plastic strain at the pipe crown. The maximum settlement was for Case J with a mere 4cm, which affects the pipe strain distribution.

Figure 11 and **Figure 12** show the pipe cross-section under the explosion for empty pipe Cases in the XY plane (Lateral Direction). While **Figure 11** shows the results for Cases A to E, **Figure 12** demonstrates the rest of the Cases. As shown in **Figure 11**, Cases A, B and C have no dent under the explosion effect. In these Cases, the groundwater table is above the pipe by at least 30cm. This resistance is due to the damping that saturated sand provides. The saturation not only makes the sand denser but also the water in its structure seems to add substantial damping. These effects help to protect the pipe. However, in Cases D and E, a dent is formed with almost 20cm and 30cm depth, respectively. These Cases are where the groundwater elevation reaches the top half of the pipe. As explained before, the soil surrounding the pipe is not fully saturated and includes both dry and saturated sand. As shown in **Figure 11**, only the pipe crown has been deformed, while the rest of the pipe remained unchanged for Cases D and E.

In **Figure 12**, in all of the shown Cases forming a dent is evident. The dent depth ranges from 30cm for Case F to nearly 35cm for Case J. The cross-section widening for Cases H, I and J is considerable. These three Cases are where the water table is below the pipe. In other words, the soil surrounding the pipe is all dry. This makes the pipe much more vulnerable, which can be seen in the widening of the pipe cross-section. After the shock reaches the pipe and pushes the crown to create a dent, the dent keeps descending with the pipe, putting more pressure on the pipe's structure. This emerges in cross-section widening as the dry soil allows this much pressure on the pipe. The cross-section widening reaches almost 13cm in Case J. The formed dent for pressurized pipe Cases was even less than 0.5cm, so their polar plots are not shown and discussed.

The pipe deformation in the YZ plane (Longitudinal Direction) for empty pipe Cases is shown in **Figures 13** (Cases A-E) and **12** (Cases F-J). By looking at these figures, other than Cases A, B and C having negligible deformations, the length of the pipe affected by the explosion in the Z-direction increases with falling groundwater table. To be precise, in Cases D and E (**Figure 13**), less than 4m of the pipe can be considered as affected length, while this length for Cases I and J is more than 8m. The fall for the point 2m away from the explosion on the pipe crown, in **Figure 14**, is less than 5cm in Cases F and G. Whereas the fall for the same point in Cases H, I and J is almost 7cm. This reinforces that the shock wave has more damaging

impacts on this buried pipe when it travels in dry sand rather than in saturated sand. As the wave propagates towards the end of the pipe, its effects are to be seen on the parts of the pipe distant from the TNT. This is why the affected length increases with the water table decreasing.

Figure 15 and **Figure 16** demonstrate the pipe effective plastic strain distribution in the section under the explosion for the empty pipe Cases. As shown in **Figure 15**, This measure for Case A reaches only 1%, while for Cases B and C, it rises to almost 2%. These plastic strains are located on the pipe crown. However, in Cases D and E, the pipe plastic strain is more than 6% in the pipe crown and almost 40 degrees away from the crown. In Case D, the effective plastic strain on the crown is almost 8% and 6% on a 40-degree section. These measures for Case E are 9% and more than 7%, respectively. These two Cases had the deepest dents, as discussed before, and the reason for this amount of plastic strain is mostly the change in soil structure close to the pipe crown. The importance of the 40-degree section is mainly due to the formed dent, as this section corresponds to where the pipe structure starts to bend and the soil structure changes. It is evident in **Figure 11** that the pipe curvature is smoother in Case D than in Case E. The groundwater difference between these two Cases explains this phenomenon.

In **Figure 16**, the shown Cases (F-J) have the effective plastic strain of more than 6.5% on the pipe crown, with Case F being the maximum of 8%. Also, other sections with 40 to 70 degrees seem to experience some fracture of the plastic strain of the pipe crown. To be precise, Case F has the effective plastic strain of almost 4% in the 50-degree section. This measure for Case G is 2.5% in the 60-degree section, and for Cases I and J, it is 2% in the 40-degree section.

Figure 17 and **Figure 18** illustrate the Von Mises stress distribution on the pipe section on the same plane as the explosion for the empty pipe Cases. By looking at **Figure 17**, it is clear that Cases A, B and C have almost uniform stress distribution over the pipe section, with almost 450MPa for Cases B and C and 200MPa for Case A. It was expected that the water table was above the pipe by a considerable margin in these Cases, which evenly distributes the explosion stress over the whole section. Conversely, in Cases D and E, Von Mises stress is considerably higher than in prior Cases, by about 400MPa. The pipe's most vulnerable points in Cases D and E are the pipe crown and an angle of 20 to 45 degrees from the crown. This stress concentration is because the water table is close to the pipe crown. In Case E, the groundwater table is almost 60 degrees from the pipe crown, where the stress on the pipe reaches 700MPa.

Figure 18 shows that the pipe crown is still the most vulnerable point in Case F with 780 MPa stress, while in the other Cases, the stress concentration can be seen on the other sides of the pipe. For instance, in Cases G and H, apart from the pipe crown, which has 500MPa stress, the same stresses can be seen at 50 to 60 degrees from the top. Also, in these Cases, the pipe's bottom part is hugely affected by the explosion to have a stress of almost H, I and J, it ranges from 150 degrees to 210 degrees. This difference is primarily due to the groundwater elevation, which in Case G, is at the bottom part of the pipe. In Cases H, I and J, the water table is completely below the pipe. So in Case G, the stress concentration is on the 120-degree section (The groundwater level), and in Cases H, I and J, it is right on the bottom part of the pipe.

The effective stress distribution over the pipe section on the explosion plane for Cases E, F and G with the pressurized pipe scenario is illustrated in **Figure 19(a)**. In this figure, the stress distribution of only these three Cases is investigated since the stress for the rest of the Cases with the pressurized pipe is lower than 50MPa. It is shown that in Case F, the Von Mises stress reaches 200MPa at an angle of 65 degrees from the pipe crown, while for Case E, it is on a 50-degree plane that the effective stress goes as high as almost 150MPa. Conversely, in Case G, the bottom half of the pipe is mostly affected by the explosion, with a stress of 150MPa on the pipe bottom.

The effective plastic strain for Cases E, F and G for pressurized pipe is shown in **Figure 19(b)**. Only these Cases are shown because the plastic strain for other Cases is negligible. Figure 19 shows the highest effective plastic strain for Case F, with only 0.23% on a 65-degree plane. This measure for Cases E and G is less than 0.15%, and its location is on a 50-degree plane and 120-degree plane, respectively. These planes are the same planes described in **Figure 19(a)**. Despite the pipe being pressurized, it seems that the groundwater depth plays an important role in stress and strain concentration on the pipe structure. As clearly understood from the results for Cases E, F and G, shown in these two figures, the same trend in the empty pipe Cases is repeated. As explained before, the depth the soil behaviour is altered tends to be a vulnerable depth for the pipe's response. Nonetheless, these measures are much lower than those of empty pipe Cases (**Figure 15-18**).

Statistical analysis is performed and shown in **Figure 20(a)** and **Figure 20(b)** regarding the ratio of pipe's diameter to burial depth being 0.813. These graphs are not limited to the pipe cross-section on the explosion plane, as in prior figures. The data for the whole pipe is used to plot these graphs.

Figure 20(a) shows the pipe's maximum effective plastic strain for different groundwater depths. By looking at it, it is clear that the internal pressure of 1MPa can reduce the pipe's effective plastic strain by a significant amount. It also shows that the maximum effective plastic strain is the highest when the

groundwater depth is at the pipe crown. At this point, a plastic strain spike gradually decreases with the groundwater depth increasing.

Figure 20(b) demonstrates the maximum effective stress for the pipe with a varying ratio of the groundwater depth to the pipe burial depth. On average, the maximum effective stress on the empty pipe is 200MPa higher than that of the pipe with 1MPa internal pressure. It also shows a stress peak when the groundwater depth reaches the pipe crown. While for the empty pipe, this peak starts at the groundwater depth to the pipe burial depth ratio of 1. For the pressurized pipe, it starts in the ratio of 1.2, which is 20 cm below the pipe crown (Case E).

6. Conclusion

The dynamic response of a buried pipe to a surface explosion with different elevations for the groundwater was elaborated using the FEM method in two scenarios: 1. Empty pipe, 2. Pipe full of water, with 1MPa internal pressure. However, this study and its results are limited to sandy soils. The points below are crucial in designing buried pipelines, although they are not considered in most of the existing buried structure codes:

1. There is a considerable stress increase of almost 25% when the groundwater depth is close to the pipe crown compared to when the groundwater table is above the pipe, whether the pipe is empty or filled with water. The stress peaks are most likely shown either on the pipe crown or at a varying angle towards the spring-line since these are the places the formed dent affects the most.

2. Having the groundwater above the buried pipe changes the deformation mode of the pipe subjected to an explosion from local (forming a dent) to non-local. This seems to be due to the stiffer soil structure where the groundwater table saturates the soil.

3. With the water table falling from the ground surface to below the buried pipe, when it is empty, the formed dent becomes deeper to the point that it almost reaches the pipe centre, where the groundwater is well below the pipe. This increases the pipe length hugely affected by the explosion and widens the pipe cross-section. Also, the contact of the groundwater with the pipe is most likely a critical point in terms of stresses and strains the pipe experiences when subjected to an explosion, whether the pipe is empty or full.

4. The internal pressure of water seems to play a protective role when the underground pipe is subjected to the explosion. This can be concluded by comparing the strains and stresses of the empty pipe and the pressurized pipe. However, amongst different Cases for water tables, for the pressurized pipe, in the Cases where the water table is in the vicinity of the pipe spring-line, the pipe has the highest strains and stresses.

7. REFERENCES

[1] Lu Y., Wang Z., and Chong K., 'A comparative study of buried structure in soil subjected to blast load using 2D and 3D numerical simulations', *Soil Dynamics and Earthquake Engineering*, vol. 25, no. 4, pp. 275–288, 2005.

[2] Fiserova D., 'Numerical analysis of buried mine explosions with emphasis on effect of soil properties on loading', 2006.

[3] Olarewaju A. J., Kameswara Rao N. S. V, and Mannan M. A., 'Blast effects on underground pipes', *Electronic Journal of Geotechnical Engineering*, vol. 15, pp. 645–658, 2010.

[4] Song K., Long Y., Ji C. et al. 'Experimental and numerical studies on the deformation and tearing of X70 pipelines subjected to localized blast loading', *Thin-Walled Structures*, vol. 107, pp. 156–168, 2016.

[5] Guo Y., Liu C., Wang D. et al. 'Numerical study and safety spacing of buried parallel gas pipelines: a study based on TNT equivalent method', *International Journal of Pressure Vessels and Piping*, vol. 168, pp. 246–257, 2018.

[6] Tang Q., Jiang N., Yao Y. et al. 'Experimental investigation on response characteristics of buried pipelines under surface explosion load', *International Journal of Pressure Vessels and Piping*, vol. 183, p. 104101, 2020.

[7] Tang Q., Jiang N., Yao Y. et al. 'Safety assessment of buried gas pipeline subject to surface explosion: A case study in Wuhan, China', *Eng Fail Anal*, vol. 120, p. 105119, 2021.

[8] Telichenko V., Rimshin V., Eremeev V. et al. 'Mathematical modeling of groundwaters pressure distribution in the underground structures by cylindrical form zone', in *MATEC Web of Conferences*, EDP Sciences, 2018, p. 2025.

[9] Zhang J., Zhang L., and Liang Z. 'Buckling failure of a buried pipeline subjected to ground explosions', *Process Safety and Environmental Protection*, vol. 114, pp. 36–47, 2018.

[10] Zhang L. and Yang X. 'Soil-tunnel interaction under medium internal blast loading', *Procedia Eng*, vol. 143, pp. 403–410, 2016.

[11] Lee W. Y., 'Numerical modeling of blast-induced liquefaction', 2006.

[12] Jayasinghe L. B., Thambiratnam D. P., Perera N. et al. 'Computer simulation of underground blast response of pile in saturated soil', *Comput Struct*, vol. 120, pp. 86–95, 2013.

[13] Lee E. L., Hornig H. C., and Kury J. W. 'Adiabatic expansion of high explosive detonation products', Univ. of California Radiation Lab. at Livermore, Livermore, CA (United States), 1968.

[14] Hallquist J. O., 'LS-DYNA theory manual', *Livermore software Technology corporation*, vol. 3, pp. 25–31, 2006.

[15] Lewis B. A., 'Developing and Implementing a Road Side Safety Soil Model into LS-DYNA', *FHWA Research and Development Turner-Fairbank Highway Research Center*, 1999.

[16] Saleh M. and Edwards L., 'Evaluation of soil and fluid structure interaction in blast modelling of the flying plate test', *Comput Struct*, vol. 151, pp. 96–114, 2015.

[17] Hallquist J. O., 'LS-DYNA keyword user's manual', *Livermore Software Technology Corporation*, vol. 970, pp. 299–800, 2007.

[18] Zhang R., Jia J., Wang H. et al. 'Shock response analysis of a large LNG storage tank under blast loads', *KSCE Journal of Civil Engineering*, vol. 22, no. 9, pp. 3419–3429, 2018.

[19] Zhang L., Liang Z., and Zhang J. 'Mechanical response of a buried pipeline to explosion loading', *Journal of Failure Analysis and Prevention*, vol. 16, no. 4, pp. 576–582, 2016.

[20] Mokhtari M. and Nia A. A., 'A parametric study on the mechanical performance of buried X65 steel pipelines under subsurface detonation', *Archives of Civil and Mechanical Engineering*, vol. 15, no. 3, pp. 668–679, 2015.

[21] Yan S., Xu Y. R., and Chang H. Y. 'Numerical simulation of dynamic response of buried pipeline by ground explosion', in *Earth and Space 2012: Engineering, Science, Construction, and Operations in Challenging Environments*, 2012, pp. 1159–1166.

[22] Souli M., Olovsson L., and Do I. 'ALE and fluid-structure interaction capabilities in LS-DYNA', in *7th International LS-DYNA Users Conference, Dearborn, Michigan*, 2002.

[23] Zhang X. L., Mi Y. M., Ji T. et al. 'Study on the Dynamic Behaviors of X70 Pipeline Steel by Numerical Simulation', in *Advanced Materials Research*, Trans Tech Publ, 2010, pp. 278–281.

[24] Wang Y.-G., Liao C. C., Wang J.-H. et al.'Dynamic response of pipelines with various burial depth due to underwater explosion', *Ocean Engineering*, vol. 164, pp. 114–126, 2018.

List of Figures

List of Tables

Table 1 Material and JWL parameters for TNT explosive [20]

ρ (kg/m^3)	v_D (m/s)	P_{CJ} (GPa)	A (GPa)	B (GPa)
1640	6930	2700	374	3.23
R_1	**R_2**	**ω**	**V**	**E_0 (GPa)**
4.15	0.95	0.3	1	7×10^9

Table 2 Parameters used in the air model [21]

ρ (kg/m^3)	$C_{0,1,2,3,6}$	C_4 (m^{-3})	C_5 (m^{-3})	E_0 (GPa)	ρ_0 (kg/m^3)
1.290	0	0.4	0.4	2.5×10^5	1.0

Table 3 Input parameters for water material model and EOS [22]

Ć(m/s)	S_1	S_2	S_3	γ_0	a	E_0(J/m^3)	V_0	ρ_0 (kg/m^3)
1480	1.75	0	0	0.28	0	0	1.0	1.025

Table 4 Simplified Johnson-Cook model parameters [23]

A′ (MPa)	B′ (MPa)	n	c	ρ (kg/m^3)	E (GPa)	ν
575	950	0.4	0.014	7850	210	0.3

Table 5 Parameters used in the dry soil model [9]

ρ (kg/m^3)	E (MPa)	μ	φ	C (KPa)
1840	20	0.3	15°	15

Table 6 Input card for the saturated sand material model [12]

ρ (kg/m^3)	G_s	ρ_{water} (kg/m^3)	N	γ	Itermax	K (Pa)	G (Pa)
1986.93	2650.0	1000	2.0	0.0001	10	5198.7	343.4
Φ_{max}	**Ahyp (Pa)**	**C (Pa)**	**e**	**A_n**	**E_t**	**m_c**	**D_1**
0.611	4.44×10^{-4}	6.2×10^{-3}	1.0	0.25	0.01	0.2521	463.0
K_{sk} (Pa)	**D_2**	**Φ_{res}**	**ε_0**	**G_f (J)**	**Damlev**	**ε_{max}**	
51.99	0	0.001	0.1	1.0×10^{-7}	0	1.0	

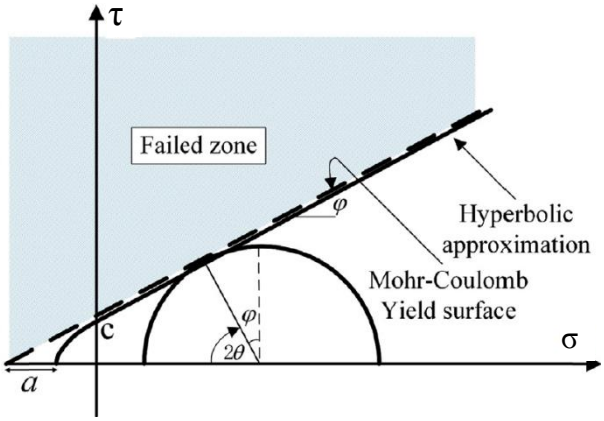

Figure 1 Mohr-Coulomb yield criterion and its hyperbolic approximation in a τ-σ plane [24].

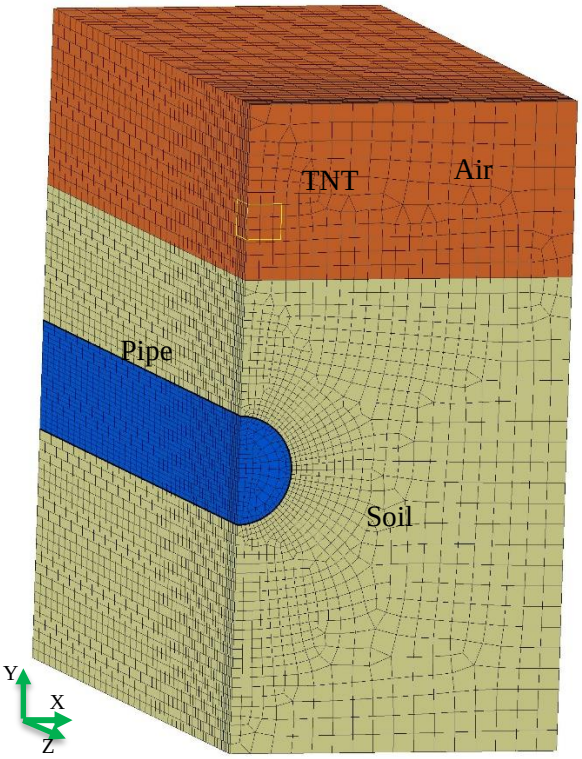

Figure 2 Schematic view of the calculated model and symmetry planes

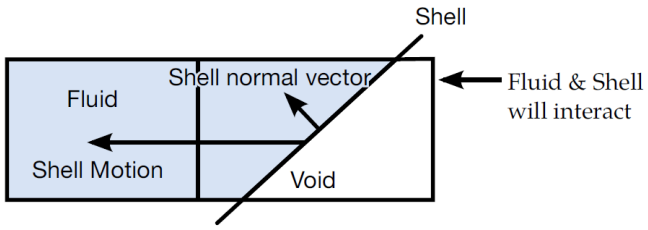

Figure 3 Shell motion in penalty-coupling algorithm

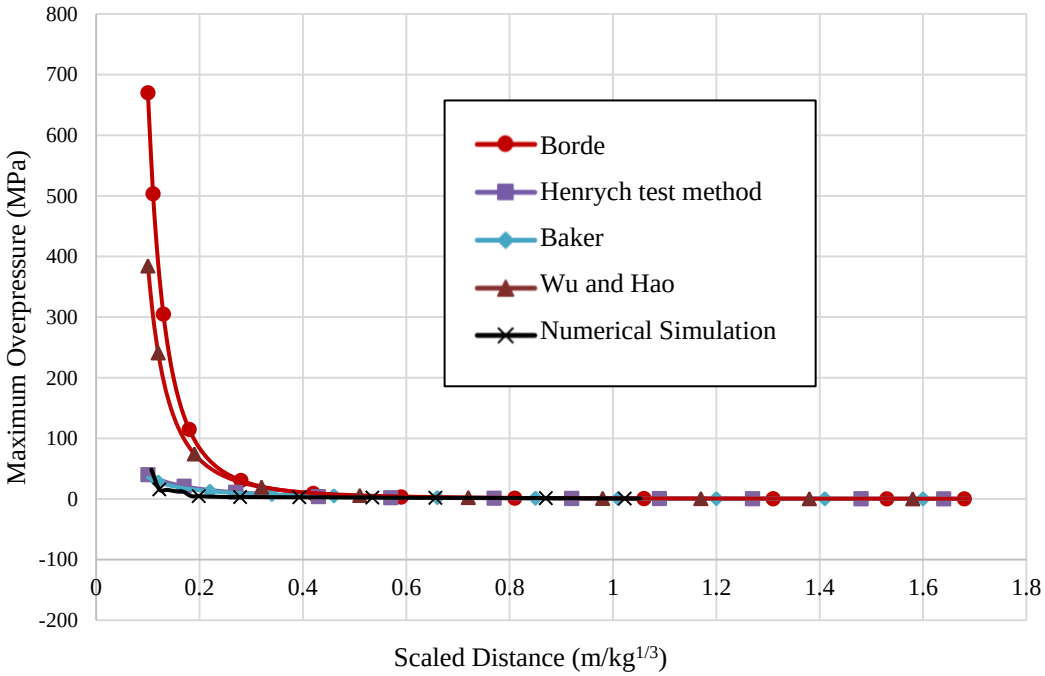

Figure 4 Comparison of the empirical formulas and the numerical results

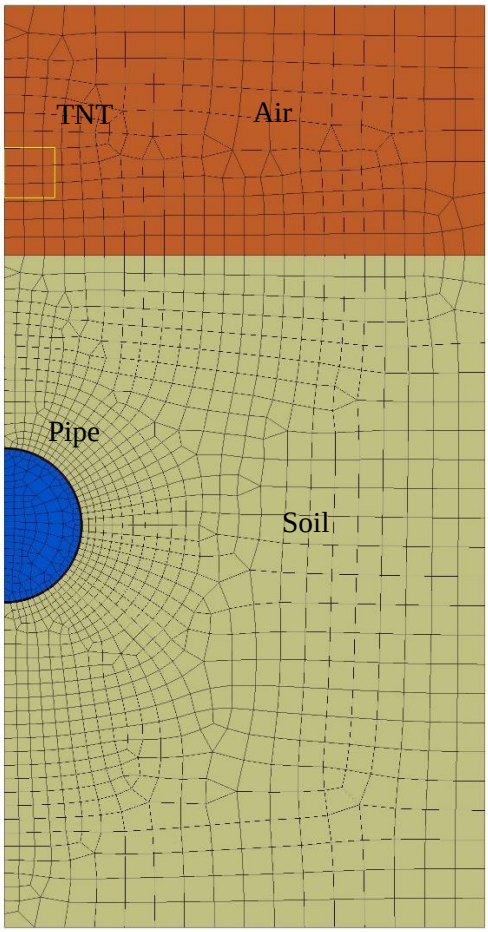

Figure 5 Geometrical model that has been used for verification.

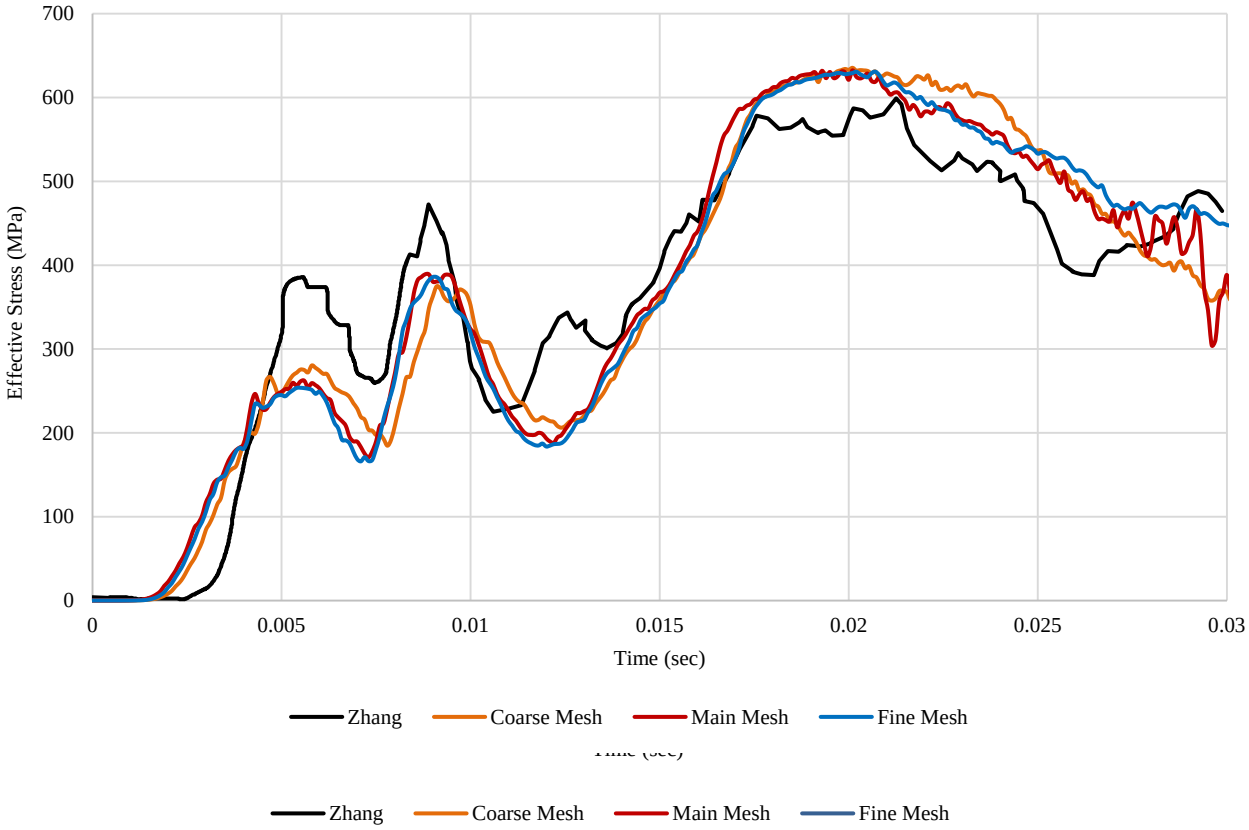

Figure 6 Model verification for the top element of the pipe.

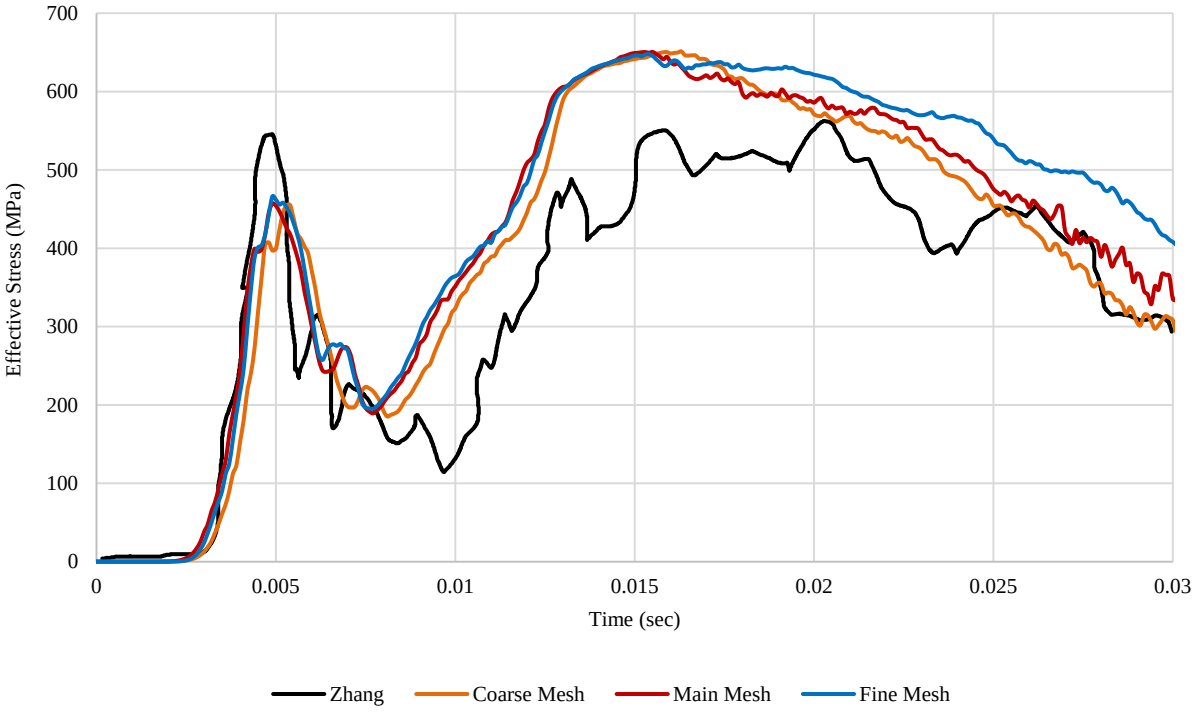

Figure 7 Model verification for the spring-line element of the pipe.

Figure 8 Model verification for the bottom element of the pipe.

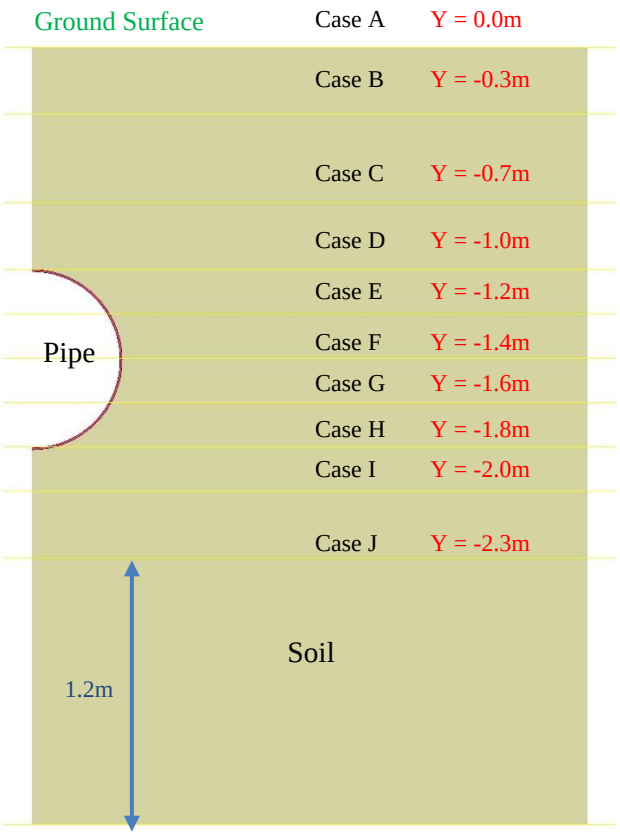

Figure 9 Different elevations considered for the water table.

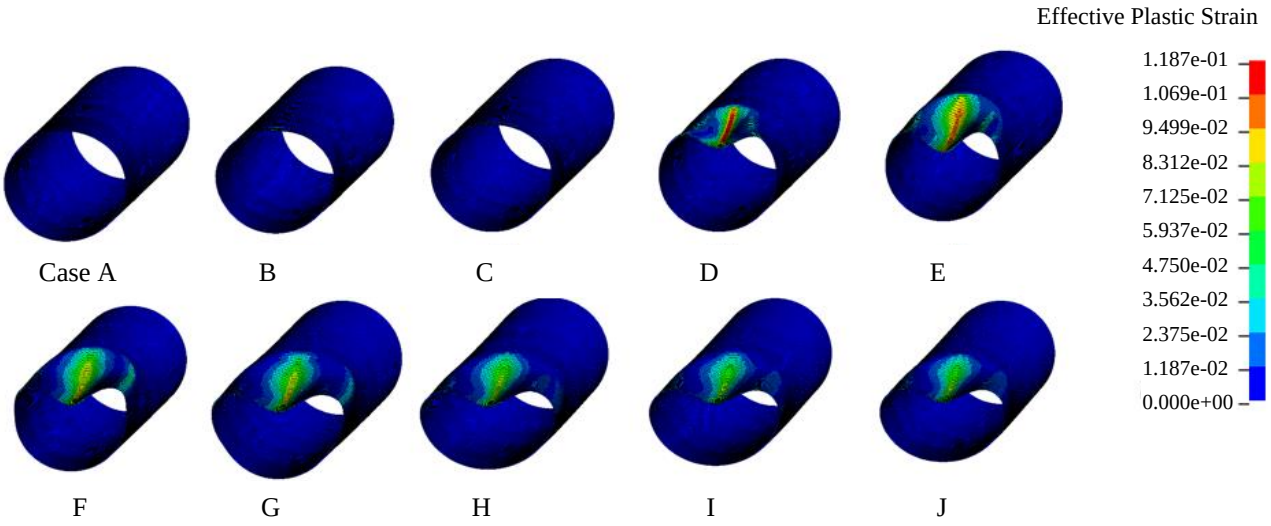

Figure 10 Maximum Effective Plastic Strain for different empty pipe Cases.

Dent Depth

Figure 11 Pipe deformation in the XY plane (Lateral Direction) for the empty pipe Cases (Cases A-E)

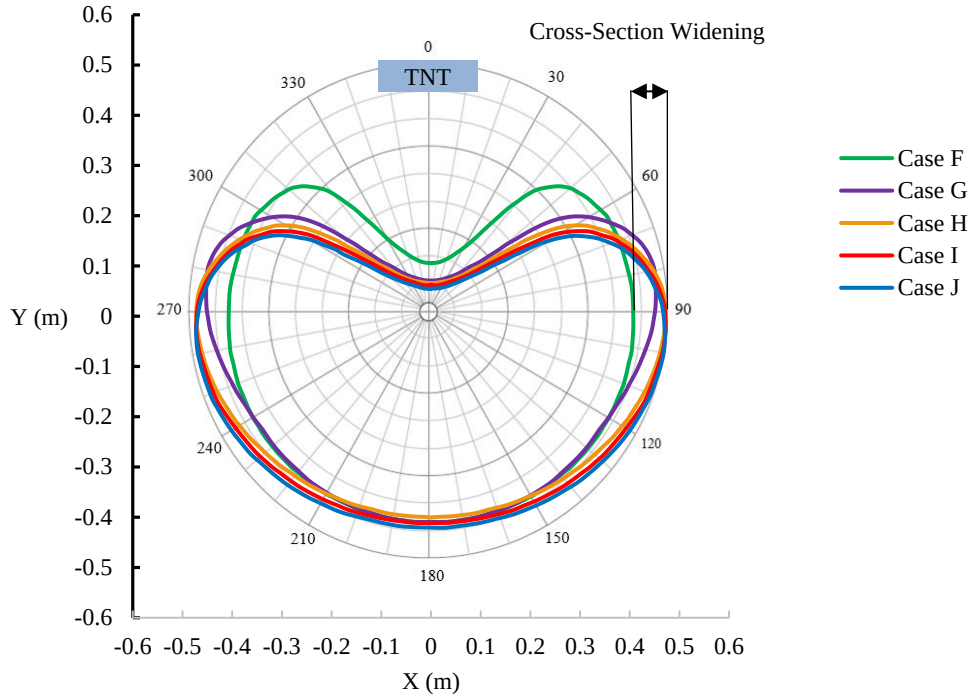

Figure 12 Pipe deformation in the XY plane (Lateral Direction) for the empty pipe Cases (Cases F-I)

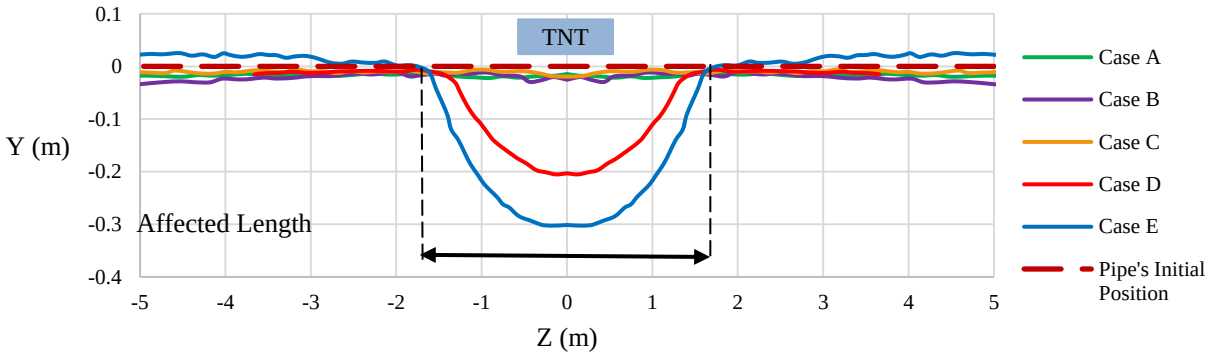

Figure 13 Pipe deformation in the YZ plane (Longitudinal direction) for the empty pipe Cases (Cases A-E)

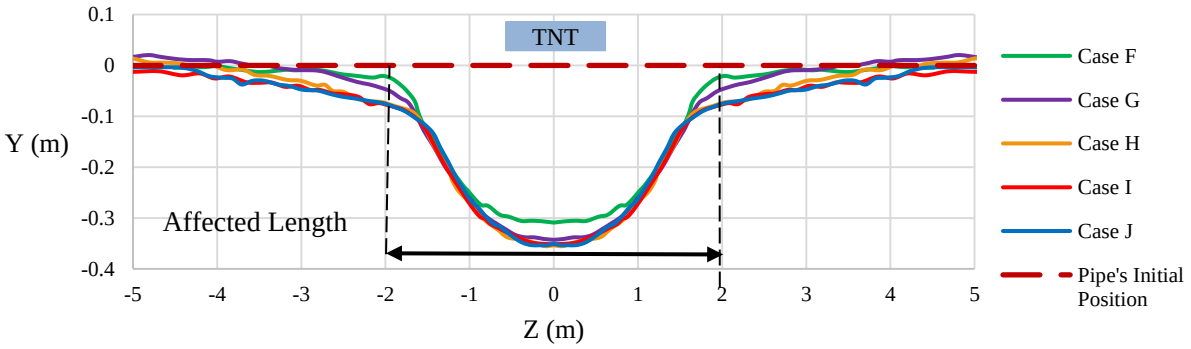

Figure 14 Pipe deformation in the YZ plane (Longitudinal direction) for the empty pipe Cases (Cases F-J)

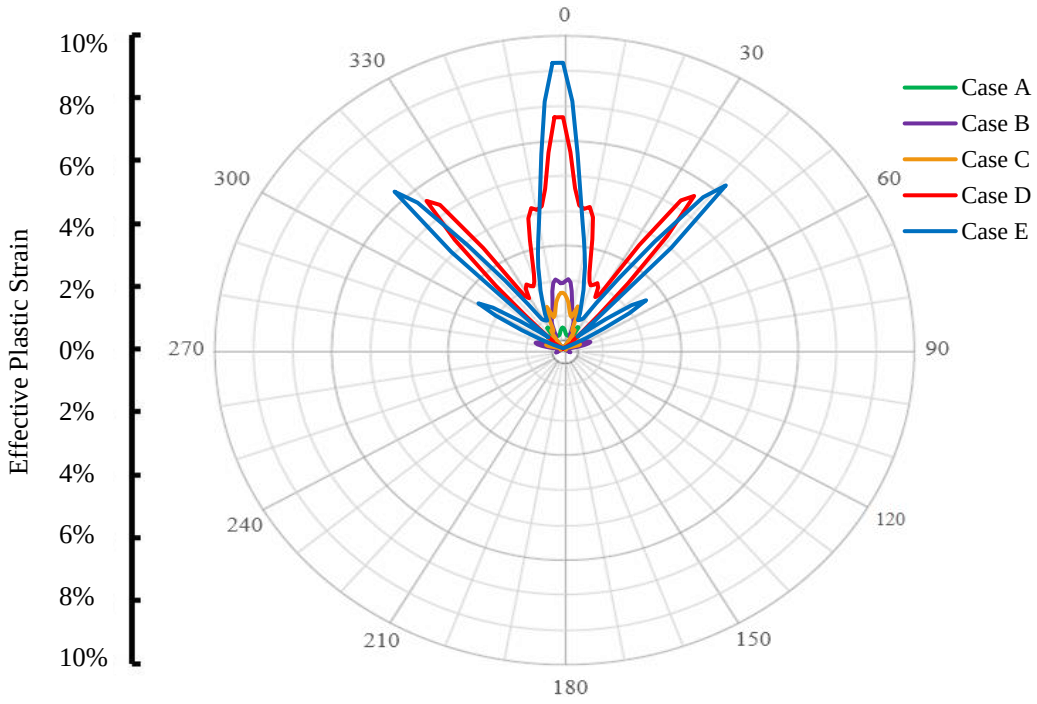

Figure 15 Effective Plastic Strain distribution for empty pipe Cases (Cases A – E)

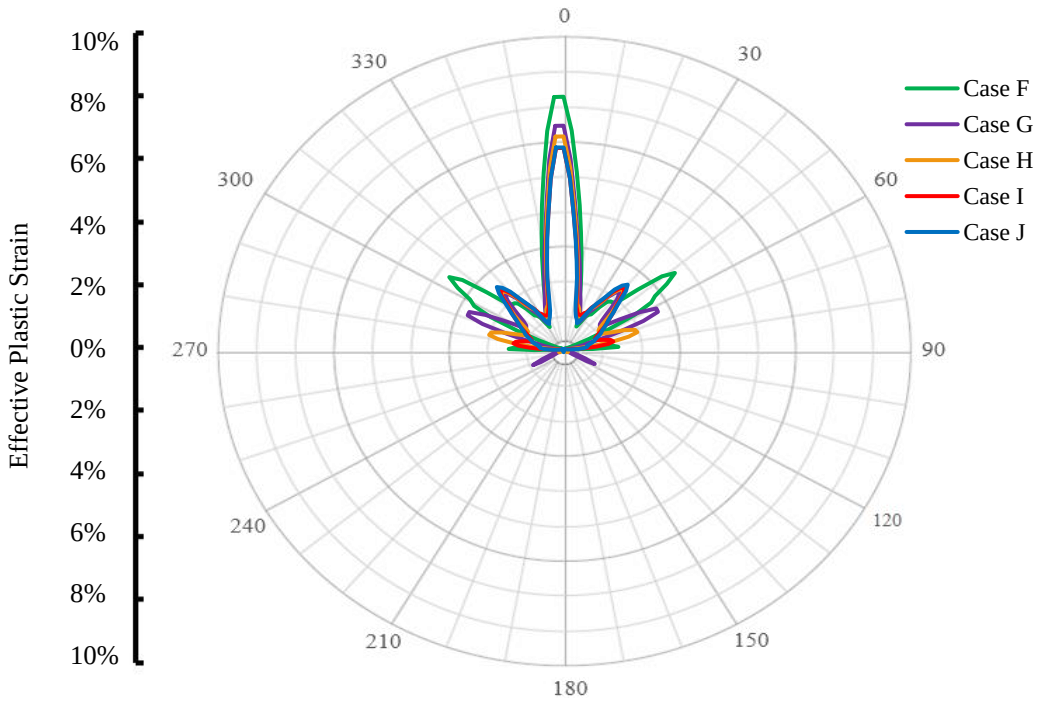

Figure 16 Effective Plastic Strain distribution for empty pipe Cases (Cases F – J)

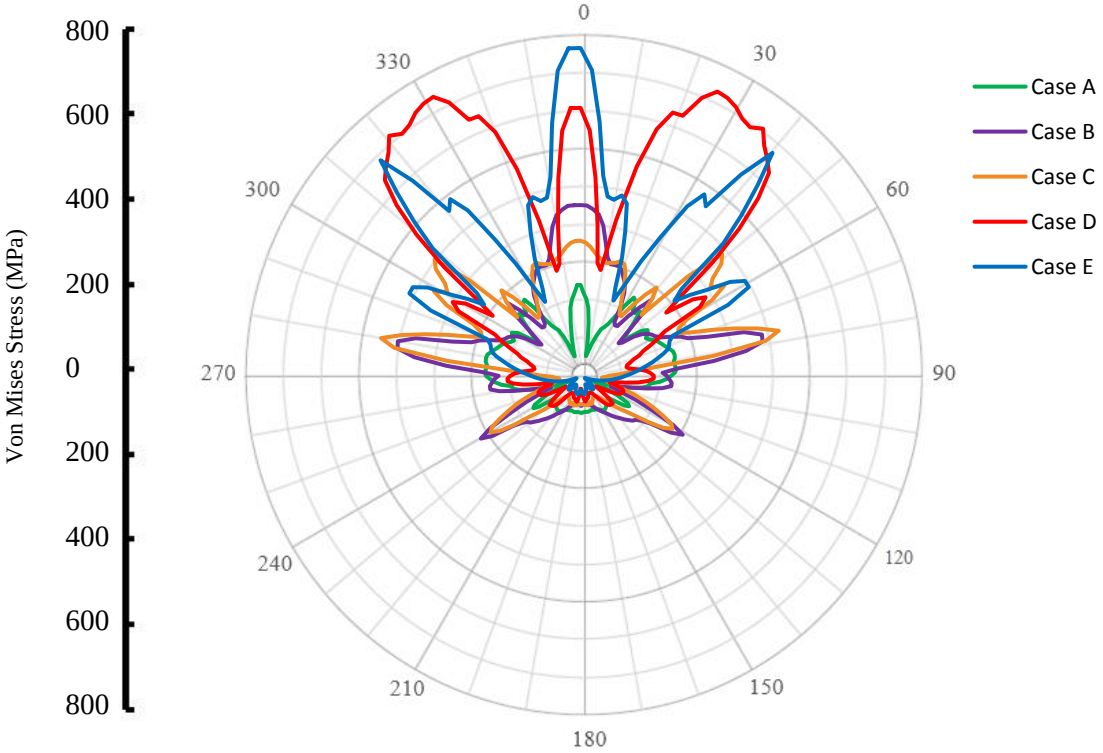

Figure 17 Von Mises stress distribution for empty pipe Cases (Cases A – E)

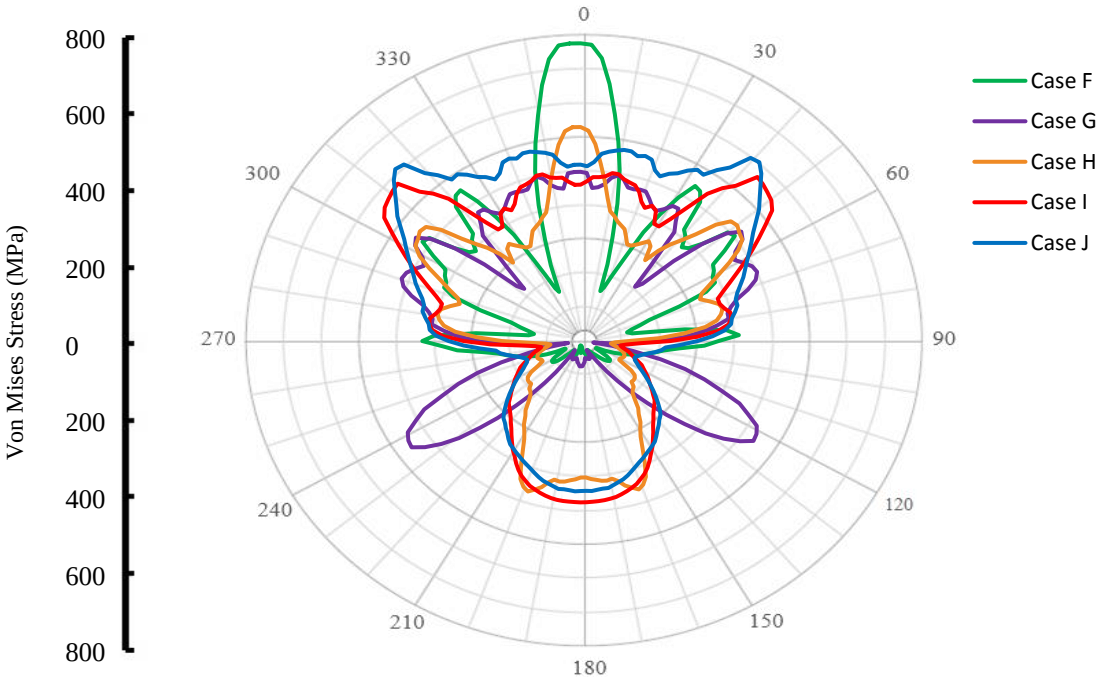

Figure 18 Von Mises stress distribution for empty pipe Cases (Cases F – J)

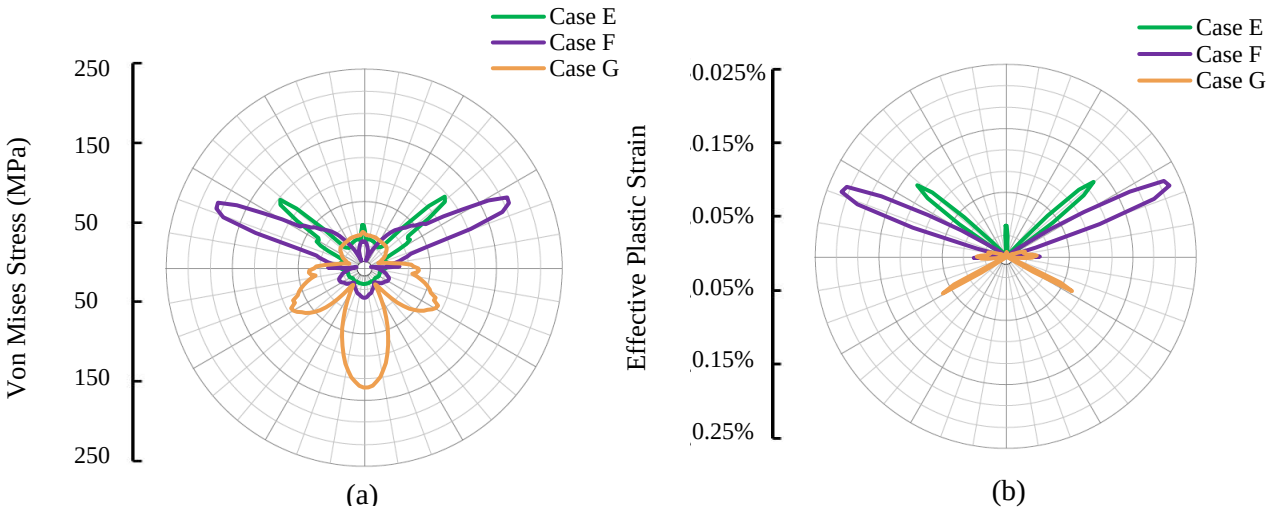

Figure 19 (a) Von Mises stress distribution and **(b)** Effective plastic strain distribution for Cases E, F and G for pressurized pipe

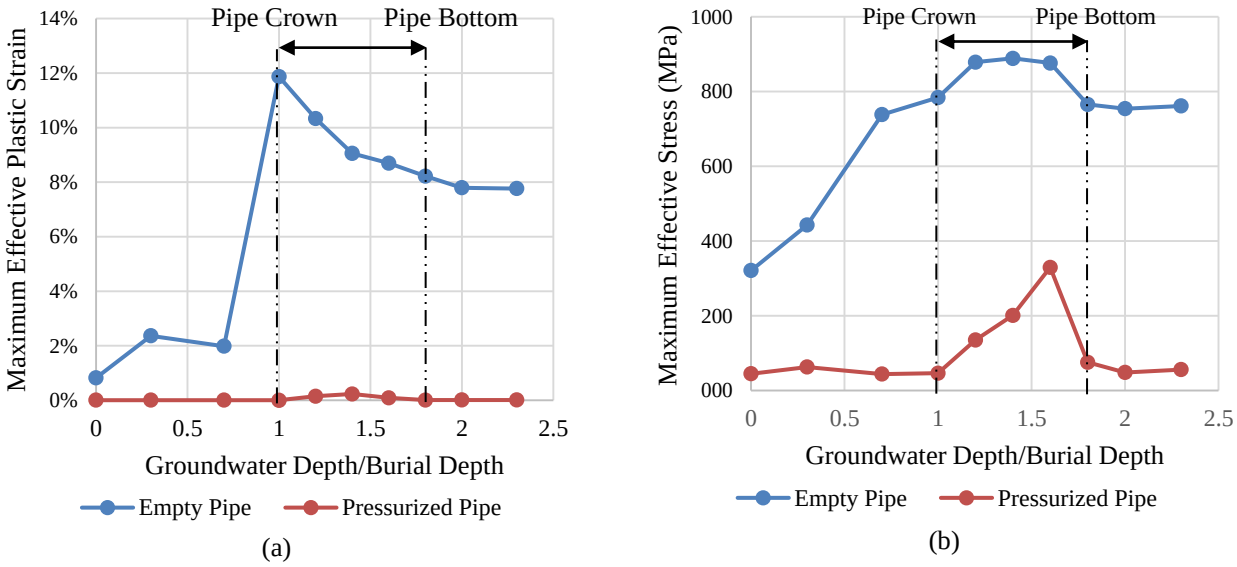

Figure 20 (a) Maximum effective plastic strain and **(b)** Maximum effective stress for the pipe with different groundwater depths

Brief Biography of the Authors

Mohammad Taghi Ahmadi is a professor of Civil Engineering at the Tarbiat Modares University, Tehran (TMU). His research field has mainly concentrated on topics of Computational Structural Mechanics, Earthquake Engineering, and Concrete Dam Analysis and Design.
Among his previous technical experiences and carriers, one should point out to; Founder and Head of the Iranian Earthquake Engineering Association, head of the Iranian National Building Code, head of the Building and Housing Research Center (BHRC), and president of TMU.
Farshid Ershadi is a master's graduate of Civil Engineering at the Tarbiat Modares University. His master's subject is Hydraulic Structures. He had his bachelor's degree in Civil Engineering from the Sharif University of Technology. His research interests are mainly Numerical Modelling, Hydraulics, Plasticity, Structural Analysis and Fluid-Structure Interaction.